Probability distribution of low-altitude propagation loss from radar sea clutter data

Peter Gerstoft and William S. Hodgkiss

Marine Physical Laboratory, University of California, San Diego, La Jolla, California, USA

L. Ted Rogers and Michael Jablecki

Atmospheric Propagation Branch, Space and Naval Warfare Systems Center, San Diego, California, USA

Received 9 April 2004; revised 13 August 2004; accepted 27 August 2004; published 11 November 2004.

[1] This paper describes the estimation of propagation loss and its statistical properties on the basis of observations of radar sea clutter data. This problem is solved by first finding an ensemble of relevant refractivity model parameters, and each refractivity model is weighted according to its data likelihood function. A parabolic equation propagation model is used both in mapping from environmental model to radar clutter data and also when mapping to propagation loss. Two different methods are then used for mapping from a statistical description of refractivity parameters to a statistical description of propagation loss. In the first approach, all of the sampled models explored in the inversion are used to give a statistical description of propagation loss. Alternatively, the environmental model is sampled from the probability for the refractivity model parameters and then mapped into propagation loss. This can be done efficiently if we are using the one-dimensional marginal distributions instead of the full distribution for the environmental parameters. *INDEX TERMS:* 3260 Mathematical Geophysics: Inverse theory; 6904 Radio Science: Atmospheric propagation; 6969 Radio Science: Remote sensing; 6982 Radio Science: Tomography and imaging; 6974 Radio Science: Signal processing; *KEYWORDS:* propagation loss estimation, radar clutter, probabilistic inversion

Citation: Gerstoft, P., W. S. Hodgkiss, L. T. Rogers, and M. Jablecki (2004), Probability distribution of low-altitude propagation loss from radar sea clutter data, *Radio Sci.*, *39*, RS6006, doi:10.1029/2004RS003077.

1. Introduction

[2] Historically, the vertical profile of atmospheric refractivity of a ''standard atmosphere'' has been used as a basis for radar performance predictions. Since the mid-1980s it has become common practice to improve this profile with surface observations of air temperature, sea temperature, wind speed and relative humidity, in conjunction with an atmospheric surface-layer model to estimate the refractivity profile within the marine atmospheric surface layer [*Liu et al.*, 1979]. The refractivity profile above the surface layer is not characterized by the surface layer models and is usually determined by weather balloons or rocketsondes [*Sylvester et al.*, 2001]. However, whereas the surface layer measurements can be made continuously, weather balloons or rocket soundings are expensive in both use of expendables and manpower. An alternative means for estimating refractivity for the purpose of radar performance assessment is to use radar clutter (e.g., Figure 1) as described by *Gerstoft et al.* [2003a, 2003b].

[3] A weakness of radar performance prediction has been the lack of a means for quantifying the impact of uncertainty in estimates of the refractivity. For example, this might be a particular concern when using radar clutter for the characterization. Consider Figure 1. A pattern of radar clutter over tens of kilometers on a given azimuth is observed. Unknown to us, however, are how random processes in individual range bins, and colored processes in range (i.e., horizontal gradients in wind speed, hence the sea clutter radar cross section) have affected the radar clutter pattern. In the context of our forward modeling, though, this makes the observation somewhat uncertain. Many different realizations of refractivity (possibly from disjoint regions in the envi-

0048-6604/04/2004RS003077$11.00

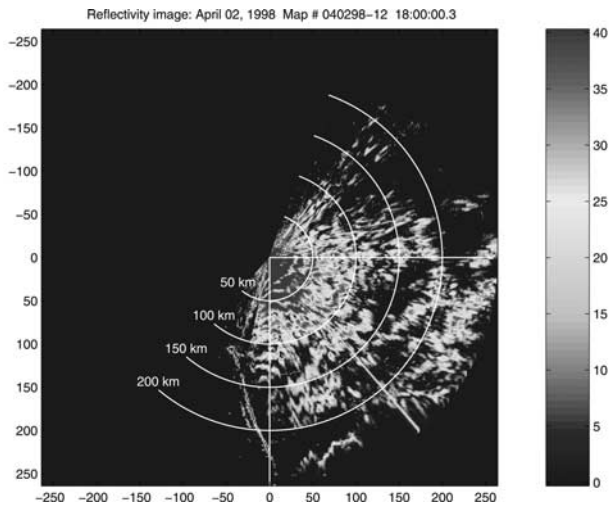

Figure 1. Clutter map (signal-to-noise ratio, measured in dB) from the SPANDAR radar corresponding to Wallops run 12. The elevation angle is 0° and E/W and N/S ranges are in kilometers. See color version of this figure at back of this issue.

ronmental parameter space) map into the region of uncertainty surrounding our observation.

[4] Previously, we have addressed the estimation of radar refractivity parameters from the Space and Range Radar (SPANDAR) [*Gerstoft et al.*, 2003a, 2003b]. An example of the received signal is shown in Figure 1, where strong clutter returns can be seen.

[5] The principle of the inversion is indicated in Figure 2. On the basis of the observed radar clutter data (the data space **d**) we statistically characterize propagation loss (the information usage domain **u**). The vector **d** represents the observed radar data at N range bins and the vector **u** represents a vector of propagation loss at certain height and range bins. As shown in Figure 2, this is mapped via a set of M refractivity parameters **m**. This involves a number of steps as outlined below:

[6] 1. Determine a model for the refractive environment [*Gerstoft et al.*, 2003a, Appendix A] and select an appropriate propagation model (e.g., TPEM [*Barrios*, 1994]). These two form the mapping **d**(**m**) from the parameter space **m** to data space **d** (see equation (6)). The vector **m** represents the unknown environmental parameters.

[7] 2. Determine the mapping **u**(**m**) from the environmental domain to usage domain. Except for a change in geometry (receiver height), here this is similar to **d**(**m**), but could be any other model (e.g. some other metric of radar performance).

[8] 3. Find acceptable models **m** from the data. As indicated in Figure 2, a region around the data can map into several acceptable solutions in the model domain.

[9] 4. Map the acceptable models into the data usage domain. Several models can map into the same usage region.

[10] As indicated in Figure 2, the mapping from data to usage domain is nonunique. There are many environmental models that give about the same goodness-of-fit. The maximum likelihood (ML) estimate of the environmental model gives the best fit. Instead of using just one estimated environment, it is proposed to describe the environmental solution probabilistically. This probability is then mapped into the usage domain. Knowing the posterior probability distribution or part thereof in the usage domain is preferable to having a single point estimate such as the usage domain result corresponding to the ML solution.

2. Inverse Problem Framework

[11] In the Bayesian paradigm, the solution to determining parameters of interest **m** given an observation **d** is characterized by the posterior probability p(**m**|**d**). First, the prior information of the model parameter vector is the probability density p(**m**). Then, this information is combined with the posterior probability p(**d**|**m**) provided by the combination of data and the physical model to give the posterior information p(**m**|**d**) of the model parameters. A clear discussion of inverse theory from a probabilistic point of view is given by *Tarantola* [1987]. Additional details of Monte Carlo sampling of posterior probabilities is given by *Sen and Stoffa* [1996], *Gerstoft and Mecklenbräuker* [1998], *Dosso* [2002], *Mosegaard and Tarantola* [2002], and *Mosegaard and Sambridge* [2002]. The solution to the inverse problem is then

$$\mathrm{p}(\mathbf{m}|\mathbf{d}) = \frac{\mathrm{p}(\mathbf{d}|\mathbf{m})\mathrm{p}(\mathbf{m})}{\mathrm{p}(\mathbf{d})}, \qquad (1)$$

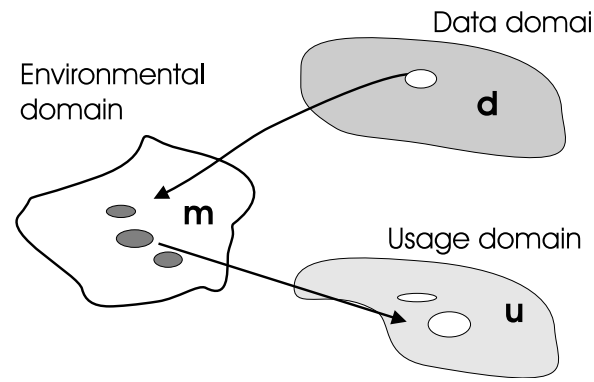

Figure 2. An observation **d** is mapped into a distribution of environmental parameters **m** that potentially could have generated it. The environmental parameters are then mapped into the usage domain **u**.

where the probability of the data p(**d**) is independent of the environmental model and here can be neglected. The posterior distribution p(**m**|**d**) contains all of the relevant information and from this distribution all relevant features of the environment can be found such as the maximum a posterior (MAP) estimator.

3. Probability of u

[12] We are not interested in the environment itself but rather better estimates in the information usage domain **u**(**m**). On the basis of the posterior distribution p(**m**|**d**), the distribution of p(**u**(**m**)) is obtained and from this distribution all relevant statistics of the usage domain can be obtained. In the present application the usage domain is propagation loss.

[13] Both the experimental data **d** and the usage domain model **u** are related to **m** via forward models $F(\mathbf{m})$ and $G(\mathbf{m})$ corresponding to **d**(**m**) and **u**(**m**). Thus formally we have $\mathbf{u} = G(F^{-1}(\mathbf{d}))$. However, this direct mapping is ill-posed and is instead interpreted probabilistically where we also can include prior information.

[14] The posterior distribution of $p_p(\mathbf{m})$ is first obtained and from this the probability distribution of **u** is obtained

$$\mathrm{p}(\mathbf{u}) = \int_{\mathcal{M}} \delta[\mathbf{u}(\mathbf{m}) - \mathbf{u}]\mathrm{p}(\mathbf{m})\mathrm{d}\mathbf{m} \tag{2}$$

where $\mathcal{M}$ represents the model space. This integral is implemented numerically, by using samples from the model space **m** based on the posterior distribution p(**m**|**d**) and then bin **u**(**m**). Two different ways to implement this mapping are suggested: 1) reusing the samples from the inversion of the data **d**, and 2) generating new samples from the probability p(**m**|**d**).

[15] 1. Reusing the samples $\{\mathbf{m}_i\}$ obtained in an inversion should be straight forward. The disadvantage of such an approach is that it has to be done following the inversion.

[16] 2. If we base the samples on the probability distribution $p(\mathbf{m}|\mathbf{d})$ then we are independent of the current inversion, and any distribution could be used. However, this requires using the full M-dimensional distribution, which apart from analytical cases is difficult to represent (assuming each parameter is described with 100 samples, then a 10-dimensional environmental model requires 10^{20} points for the full probability distribution). If we neglect all parameter correlations in the posterior distribution then

$$\mathrm{p}(\mathbf{m}|\mathbf{d}) = \prod_j^M \mathrm{p}(m_j) \tag{3}$$

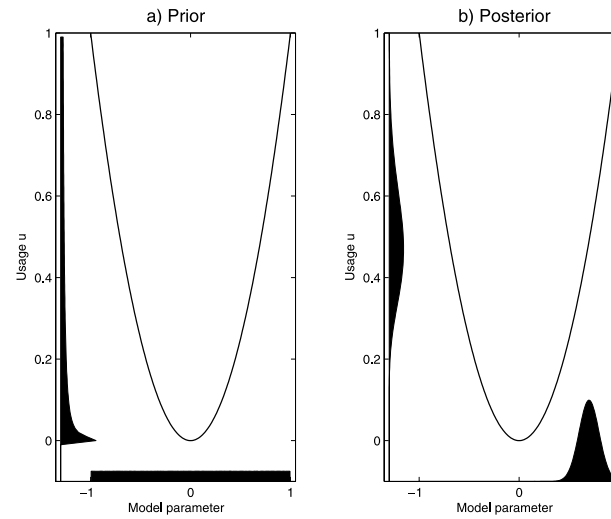

Figure 3. Mapping from model parameter probability p(m) to usage probability p(u) for (a) prior and (b) posteriori knowledge. The mapping is here $u = f(m) = m^2$. The distribution on the x axis shows the probability for the model parameter p(m) and the distribution on the y axis the probability for the usage domain p(u).

Thus we can generate samples $\mathbf{m}_i$ from the M marginal distributions p(m_j) for each parameter m_j. This is computationally very efficient, but can lead to biases in the solution for correlated parameters.

[17] From the distribution p(**u**) all relevant statistical features of the usage domain, e.g., propagation loss, can be obtained, as for example the mean and variation of **u**

$$\mathsf{E}[\mathbf{u}] = \int \mathbf{u}'\mathrm{p}_p(\mathbf{u}')\,\mathrm{d}\mathbf{u}' \tag{4}$$

$$\mathsf{Var}[\mathbf{u}] = \int (\mathbf{u}') - \mathsf{E}[\mathbf{u}])^2\mathrm{p}_p(\mathbf{u}')\mathrm{d}\mathbf{u}' \tag{5}$$

[18] In the environmental model space the posterior distribution p(**m**|**d**) usually is more narrow than the prior distribution p(**m**). This is because the data **d** contains information which causes the posterior distribution to be more narrow as seen from equation (1). This is not necessarily the case for the usage distribution p(**u**) as illustrated by the simple example in Figure 3 and further discussed in section 5.

[19] The simple example, Figure 3, shows for a synthetic mapping from model to usage domain, $u = f(m) = m^2$. The uniform prior model p(m) in Figure 3a gives a relatively concentrated usage distribution p(u), whereas the more narrow prior in Figure 3b gives a less

concentrated usage distribution. With nonlinear mappings it is not known if the posterior p(u) will be more narrow than the prior.

4. Likelihood and Objective Function

[20] The likelihood and the objective function are derived assuming a simple linear model

$$\mathbf{d} = S\mathbf{d}(\mathbf{m}) + \mathbf{e}. \tag{6}$$

the scalar S represents unknown radar strength and calibration constants. $\mathbf{d}$ and $\mathbf{d}(\mathbf{m})$ represents measured and modeled data organized into a vector of N data points, corresponding to each range bin; $\mathbf{m}$ represent the M environmental parameters to be determined. Assume the errors $\mathbf{e}$ to be Gaussian distributed with mean $S\mathbf{d}(\mathbf{m})$ and covariance $\mathbf{C}$. The errors represent all features that are not modeled in the data as noise, theoretical errors, and modeling errors.

[21] The likelihood function is

$$L(\mathbf{m}) = (\pi|\mathbf{C}|)^{-N} \exp\Big(-[\mathbf{d} - S\mathbf{d}(\mathbf{m})]^{\mathrm{T}}\mathbf{C}^{-1}[\mathbf{d} - S\mathbf{d}(\mathbf{m})]\Big). \tag{7}$$

where N is the number of data points. For convenience, although strictly speaking not true, we assume $\mathbf{C} = \nu\mathbf{I}$. The source S can be estimated in closed form by requiring $\partial \log L/\partial S = 0$, whereby

$$S^{\mathrm{ML}} = \frac{\mathbf{d}^{\mathrm{T}}\mathbf{d}(\mathbf{m})}{\| \mathbf{d}(\mathbf{m}) \|^2} \tag{8}$$

It is seen that S depends on $\mathbf{m}$ but not on ν. The likelihood function is then

$$L(\mathbf{m}) = (\pi\nu)^{-N} \exp(-\phi(\mathbf{m})/\nu) \tag{9}$$

where

$$\phi(\mathbf{m}) = \mathbf{d}^2 - \left(\frac{\mathbf{d}^{\mathrm{T}}\mathbf{d}(\mathbf{m})}{\| \mathbf{d}(\mathbf{m}) \|}\right)^2, \tag{10}$$

is the objective function. The likelihood estimate of the noise ν^{ML} can be estimated in closed form by solving $\partial \log L/\partial\nu = 0$,

$$\nu^{\mathrm{ML}} = \phi(\mathbf{m})/N. \tag{11}$$

Reinserting this into the likelihood function gives

$$L(\mathbf{m}) = \left(\frac{N}{\pi e \phi(\mathbf{m})}\right)^N. \tag{12}$$

[22] The ML solution $\mathbf{m}^{\mathrm{ML}}$ is obtained by maximizing the objective function over all $\mathbf{m}$. Finally, an overall estimate for the error power ν is obtained from (11) at the environmental ML solution: $\nu^{\mathrm{ML}}(\mathbf{m}^{\mathrm{ML}})$ and can be reinserted into the likelihood function. For simplicity, we consider the error as known and only keep the free argument $\mathbf{m}$ of the objective function ϕ. This approach leads to [*Gerstoft and Mecklenbräuker*, 1998]

$$L(\mathbf{m}) = \left[\frac{N}{\pi\phi(\mathbf{m}^{\mathrm{ML}})}\right]^N \exp\left[-N\frac{\phi(\mathbf{m})}{\phi(\mathbf{m}^{\mathrm{ML}})}\right]. \tag{13}$$

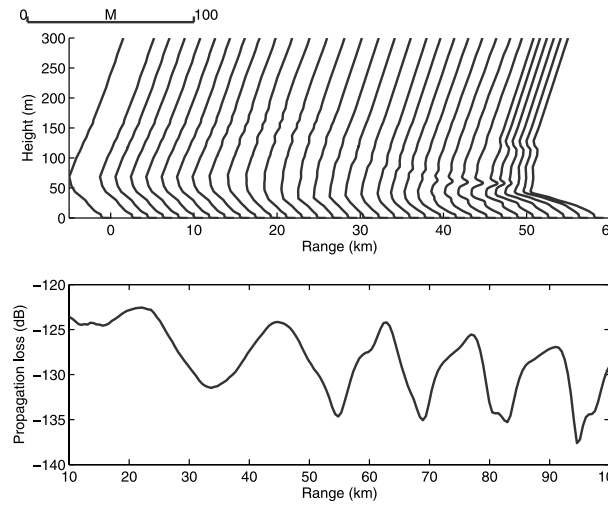

Figure 4. The refractivity profile (top) used to generate the data and (bottom) the propagation loss data.

[23] The above derivation assumes that the error in each sample is uncorrelated with the next sample. In practice these are strongly correlated because both the radar clutter cross section and also the modeling error due to wrong parameterizations or wrong parameter values varies slowly with range. Therefore the number of samples N in the above equations must be replaced with the effective number of samples, N_{eff}.

5. Example

[24] The data are generated based on the helicopter measured range-dependent refractivity profiles (run 7) for the Wallops 98 experiment [*Gerstoft et al.*, 2003a], as shown in Figure 4. These profiles were interpolated using the LARRI program [*Konstanzer*, 1999].

[25] These profiles are bilinear. However, our parameterization of the environment is trilinear and is able to capture both this type of environment as well as a trilinear environments typical of the Southern California basin.

[26] The propagation loss in a range interval from 10–100 km is then used. A simple trilinear model is used for

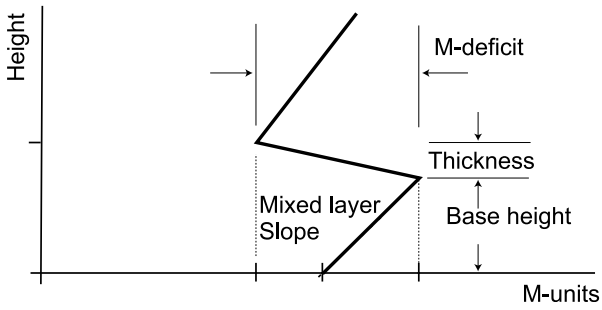

Figure 5. Trilinear profile for the refractivity.

the refractivity profile as outlined in the work of *Gerstoft et al.*, 2003a, Appendix A], see Figure 5. We then search for refractivity parameters at both 0- and 100-km range with the unknown parameters and their search range as given in Table 1. Thus we have 8 unknown parameters for the refractivity profile. To obtain refractivity profiles at other ranges the parameters are interpolated linearly. The first 3 parameters were given a uniform distribution but the slope was given a nonuniform distribution as indicated in Figure 6. This constraint is implemented by giving the slope a uniform distribution that depends on base height, $U[0.13; (0.13 - 1.13 * \exp(-h/110)]$, where h is the base height in meters (the base height was given a uniform distribution). In the above formula 0.13 corresponds to standard atmosphere.

[27] The reason for the nonuniform distribution for the slope is based on *Gossard and Strauch* [1983] and *Brooks et al.* [1999]. They describe the evolution of ducts associated with (thermal) internal boundary layers. These ducts form when a warm and dry terrestrial boundary layer flows out over cool water leading to an internal boundary layer forms between them. Particularly near the shore, the layer is shallow (on the order of a few to several 10s of meters), stably stratified and the humidity gradient in the internal boundary is negative. The associated modified refractivity gradient is negative as well. As we go out in range, stable stratification gives way to the formation of a surface layer, a mixed layer and a capping inversion. This boundary layer is deeper (say 50 m to 200 m or more), and resembles the ducting structure associated with a subsidence driven inversion such as is often seen in the southern California bight. With these deeper structures having a real mixed layer, the negative gradients of refractivity are confined to the surface layer (as described by Monin Obukhov theory) and the capping inversion.

Table 1. Inversion Model With Parameter Search Bounds[a]

Model Parameter	Lower Bound	Upper Bound
Base height, z_b, m	0	400
M deficit, M_d, M units	0	250
Thickness, z_{thick}, m	0	150
Slope, M units/m	−1	0.13
Evaporation duct height, m	0	50

[a]These parameter bounds were used both at the initial range ($r = 0$) and at the final range ($r = 100$ km). For all ranges each parameter was linearly interpolated.

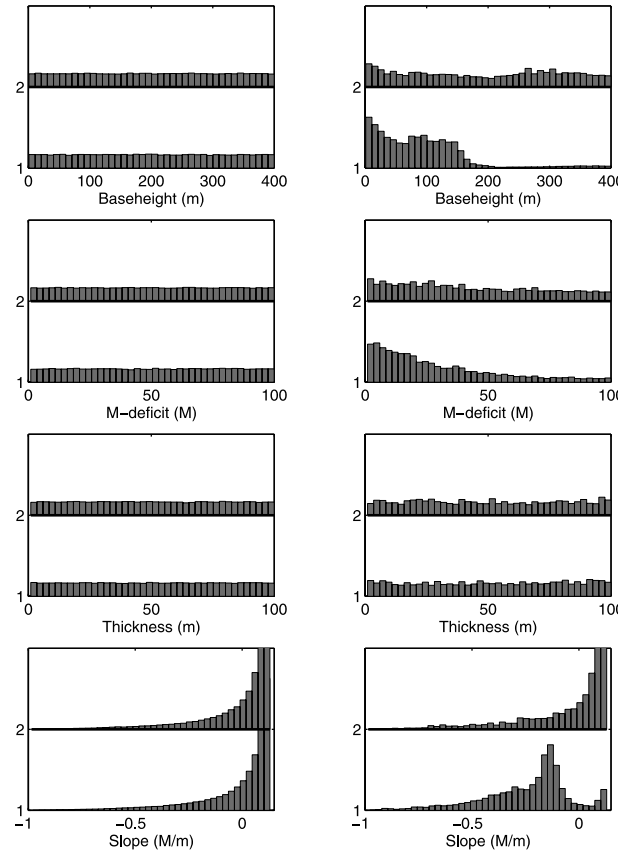

Figure 6. (left) Prior and (right) posterior distributions of the parameter estimates. The "1" and "2" refer to the parameters at the 0- and 100 km-range, respectively.

5.1. Refractivity Estimation

[28] Using this environmental model, 90,000 replicas are precomputed. To compute the prior distribution of the environmental parameters all samples are weighted evenly (Figure 6). The smoothness of these indicate that the prior is well sampled. To compute the posterior distribution (Figure 6), equations (1) and (13) are used. We note that the overall behavior seems reasonable, as the distributions are smooth and the peaks are at reasonable values. A more robust convergence criterion might indicate that the distributions are not yet completely converged. This could for example be done by

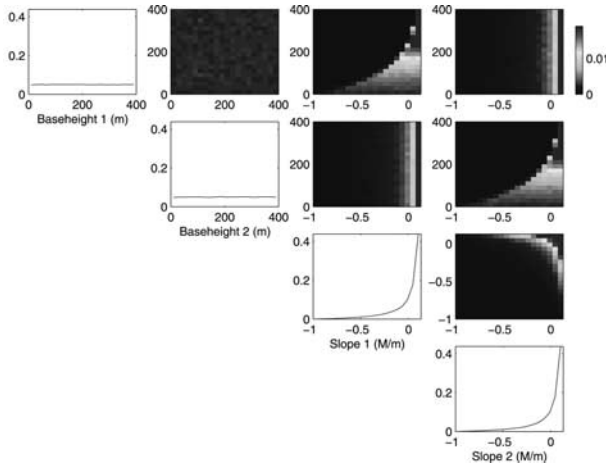

Figure 7. Prior probability distribution for the base height and slope at 0- and 100-km range. Along the diagonal the marginal for each parameter is plotted and above the diagonal show the 2-D marginals (red indicates higher probability). The distributions below the diagonal are symmetric with those above. See color version of this figure at back of this issue.

requiring two independent estimates of the probabilities to converge to the same distribution [*Dosso*, 2002].

[29] The 1-D and 2-D prior marginals for base height and slope are shown in Figure 7. The 2-D marginals between base height and slope at the same range show clearly the restriction of no negative slopes for large base height. The other marginals are uncorrelated. For the posterior 1-D and 2-D marginals, Figures 6 (right) and 8, the data has caused the posterior distribution for the slope to move to slightly negative slopes.

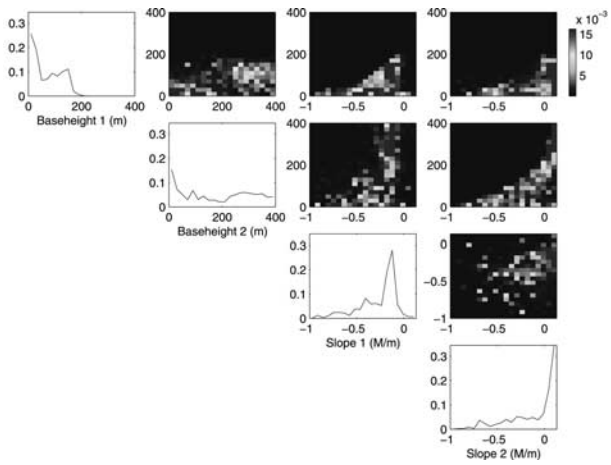

Figure 8. Posterior probability distribution for the base height and slope at 0- and 100-km range. Along the diagonal the marginal for each parameter is plotted and above the diagonal show the 2-D marginals (red indicates higher probability). The distributions below the diagonal are symmetric with those above. See color version of this figure at back of this issue.

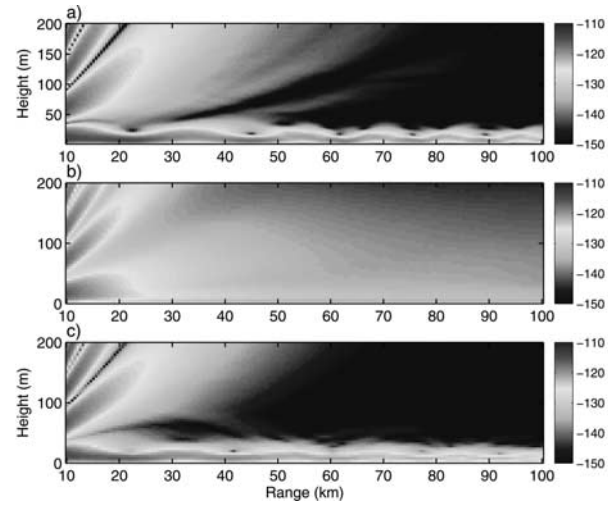

Figure 9. The propagation-loss field based on (a) the true environment (from Figure 4a), (b) prior information, and (c) posteriori information (bottom). See color version of this figure at back of this issue.

5.2. Estimating Propagation Loss

[30] An important issue is to be able to estimate statistics of posterior propagation loss. Figures 9–16 illustrate this estimation. The posterior probability dis-

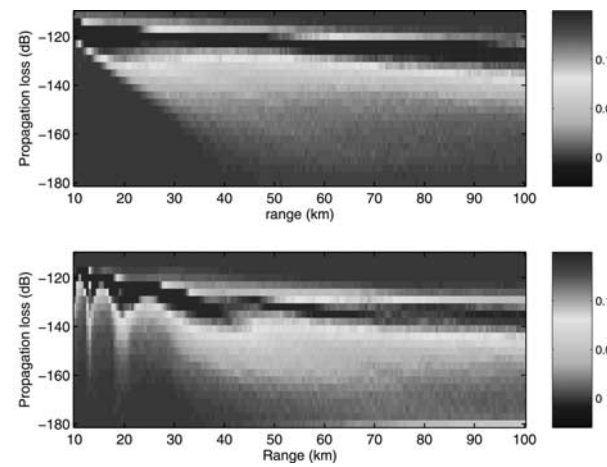

Figure 10. Prior probability distribution for propagation loss versus range at (top) 12-m and (bottom) 104-m height. See color version of this figure at back of this issue.

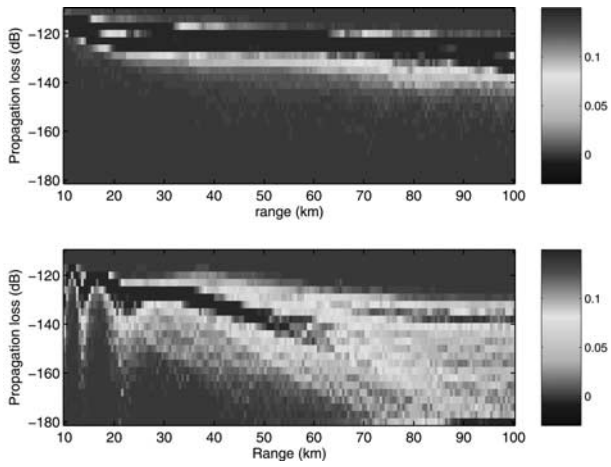

Figure 11. Posteriori probability distribution for propagation loss versus range at (top) 12-m and (bottom) 104-m height. See color version of this figure at back of this issue.

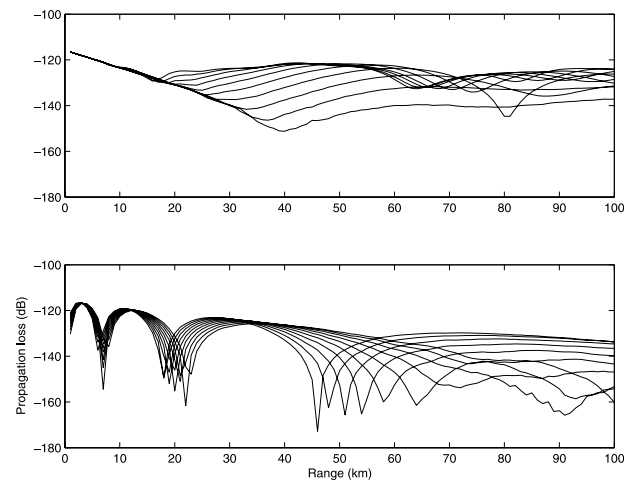

Figure 13. Variation in propagation loss at (top) 12 m and (bottom) 104 m as the M deficit is changed from 5 to 25 M units in a 50-m-high duct.

tribution of the propagation loss is based on weighting the propagation loss from each refractivity model with the posterior probability, equation (2). We will use both Approach 1 (using inversion samples) and Approach 2 (based on the 1-D marginals of the distribution). Since Approach 1 captures directly the interrelation between the parameters we emphasize that approach.

5.2.1. Propagation Loss From the Inversion Samples

[31] Here we use the samples and their associated likelihood from the data inversion (Approach 1 in section 3). We compute the posterior propagation loss based on a weighting of the propagation loss from each generated refractivity model.

[32] First we compute the propagation loss based on the true environment, Figure 9a. The average prior propagation loss, that is computing the propagation loss as a sample mean over all propagation losses for each of the refractivity models is shown in Figure 9b. The average posterior propagation loss is shown in Figure 9c, that is the same as the prior but weighted with likelihood function for each environmental model. It is seen that the posterior propagation loss identifies a ducting environment as observed in the data, Figure 9a, but the prior does not.

[33] The probability distribution of the field then is computed. Both prior field (Figure 10) and the posterior field (Figure 11) are calculated at 12- and 104-m height as a function of range. At 104-m height and ranges larger

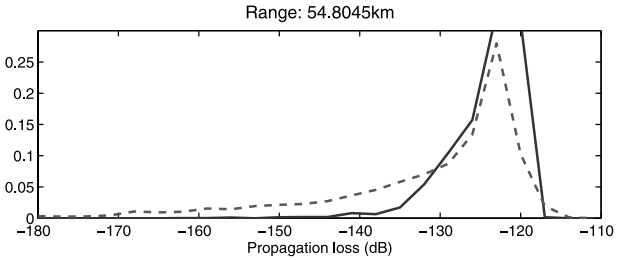

Figure 12. Posteriori (solid curve) and prior (dashed curve) probability at 50-km range and 12-m height.

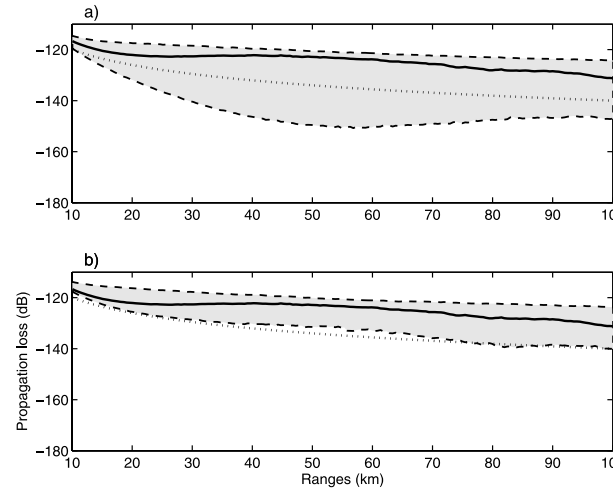

Figure 14. The median field (solid curve) and the 10th and 90th percentile (both dashed curves) at 12-m height (dashed) based on all (a) prior samples and (b) posteriori samples. The gray area indicates the range between the 10th and 90th percentile. For reference, a r^{-1} decay (dotted) is shown on each plot.

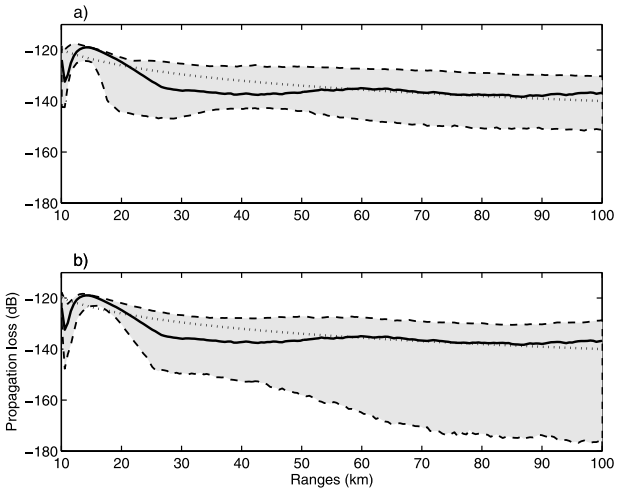

Figure 15. The median field (solid) and the 10th and 90th percentile (both dashed) at 104-m height (dashed) based on all (a) prior samples and (b) posteriori samples. The gray area indicates the range between the 10th and 90th percentile. For reference a r^{-1} decay (dotted) is shown on each plot.

than about 60 km it is seen that the propagation loss can be quite large and this is the reason for the large concentration at −180 dB, corresponding to a receiver located in the shadow zone above the duct. Figure 12 shows the probability distribution at 50-km range and 12-m height. This corresponds to a simple vertical cut at 50-km range though the contour plots in Figures 10 and 11.

[34] It is interesting to notice that the posterior propagation loss at 104-m height (Figure 11) is more uncertain than the prior propagation loss (Figure 10). Often the posterior is more certain than the prior, as is the case at 12-m height, but as argued in connection with Figure 3 this may not be the case. The reason that it is more narrow at 12 m is due to the duct. As long as the receiver is in the duct there is not much fluctuation in the strength of the field, see Figure 13. For a receiver above the duct there is huge variation depending on how the energy escapes the duct.

[35] On the basis of the distribution of propagation loss p(**u**), the median and 10- and 90-percentiles are computed as a function of range (10–100 km) in the duct (12-m height, Figure 14) or above the duct (104-m height, Figure 15). As we have the full distribution it is preferable to characterize it with median and percentiles instead of mean and standard deviations. Since the distributions are not symmetric around the median neither are the percentiles. Clearly, the posteriori distribution is much more compact for the lower height than for the higher height; a behavior that is expected given that the input data is effectively related to the propagation loss at the surface. The range between the 10th and the 90th percentiles at 104-m height shows a wider posterior than prior, this has been explained in the discussion related to Figures 10 and 11.

5.2.2. Propagation Loss From Environmental Probabilities

[36] Here we assume that the posteriori probabilities p(**m**|**d**), are fully described by their 1-D marginal distributions (Figure 6, right) and then sample refractivity profiles and their propagation loss using Monte Carlo integration (Approach 2 in section 3).

[37] If the parameters are strongly correlated then the full probability density function is not well represented by the product of the 1-D marginals (equation (3)) and the estimated probability for propagation loss will be less accurate. As can be seen in Figure 8 there is some cross correlation between the parameters, so we are violating the assumption that each parameter is independent. However, the estimated posterior probabilities using this method (Figure 16) are similar to the ones using the full distribution (Figure 11), although there is slight difference in the details. In this case, just using the 1-D marginals to compute posterior propagation loss gives satisfactory results.

6. Conclusion

[38] An algorithm for estimating the statistical properties of propagation loss based on the refractivity from radar clutter has been described using a likelihood formulation. Refractivity from radar clutter refers to an

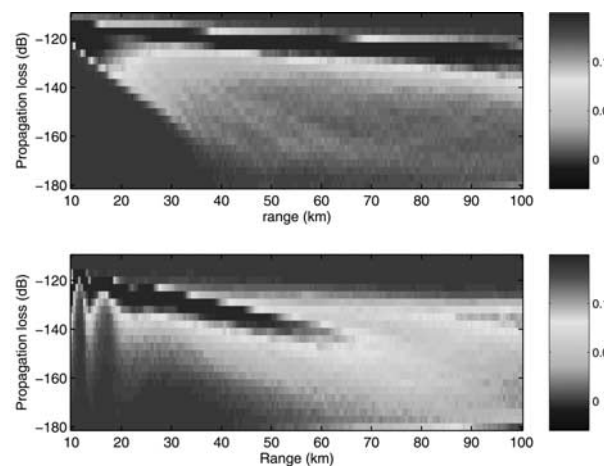

Figure 16. Posteriori probability distribution for propagation loss versus range at (top) 12-m and (bottom) 104-m height based on the 1-D marginal posterior parameter distribution in Figure 6. See color version of this figure at back of this issue.

inversion approach whereby information in a radar return is transformed into estimates of refractivity parameters. The approach taken here then maps the refractivity and their uncertainties into propagation loss. The likelihood function is developed assuming the error in the data is Gaussian.

[39] Two methods were used for generating the posterior propagation loss. The first method was based directly on the environmental samples from the inversion weighted with the likelihood. In the second, random samples were selected from the 1-D marginal probability distributions of the environmental parameters.

[40] The second approach has the advantage that it is independent of the inversion and easily could be generalized to include other types of information (e.g., from numerical weather predictions).

[41] It also assumes that the marginal probability distributions are independent. For strongly coupled parameters this will not be the case and it potentially can give biased results, but we have not yet investigated this problem.

[42] **Acknowledgment.** This work was funded by the Office of Naval Research under grant N00014-03-1-0393.

References

Barrios, A. E. (1994), A terrain parabolic equation model for propagation in the troposphere, *IEEE Trans. Antennas Propagat.*, *42*(1), 90–98.

Brooks, I. M., A. K. Goroch, and D. P. Rogers (1999), Observations of strong surface radar ducts over the Persian Gulf, *J. Appl. Meteorol.*, *38*, 1293–1310.

Dosso, S. E. (2002), Quantifying uncertainties in geoacoustic inversion. I. A fast Gibbs sampler approach, *J. Acoust. Soc. Am.*, *111*(1), 129–142.

Gerstoft, P., and C. F. Mecklenbräuker (1998), Ocean acoustic inversion with estimation of a posteriori probability distributions, *J. Acoust. Soc. Am.*, *104*(2), 808–817.

Gerstoft, P., L. T. Rogers, J. L. Krolik, and W. S. Hodgkiss (2003a), Inversion for refractivity parameters from radar sea clutter, *Radio Sci.*, *38*(3), 8053, doi:10.1029/2002RS002640.

Gerstoft, P., L. T. Rogers, W. S. Hodgkiss, and L. J. Wagner (2003b), Refractivity estimation using multiple elevation angles, *IEEE Oceanic Eng.*, *28*(3), 513–525.

Gossard, E. E., and R. G. Strauch (1983), *Radar Observations of Clear Air and Clouds*, Elsevier Sci., New York.

Konstanzer, G. C. (1999), Large-scale Atmospheric Refractivity Range Interpolator (LARRI), paper presented at URSI National Radio Sciece Meeting, Union Radio Sci. Int., Boulder, Colo., 4–7 Jan.

Liu, W. T., K. B. Katsaros, and J. A. Businger (1979), Bulk parameterization of air-sea exchanges of heat and water vapor including molecular constraints on the interface, *J. Atmos. Sci.*, *36*, 1722–1735.

Mosegaard, K., and M. Sambridge (2002), Monte Carlo analysis of inverse problems, *Inverse Probl. Opt.*, *18*(3), 29–54.

Mosegaard, K., and A. Tarantola (2002), Probabilistic approach to inverse problems, Chapter in *International Handbook of Earthquake and Engineering Seismology*, edited by W. H. K. Lee et al., pp. 237–265, Academic, San Diego, Calif.

Sen, M. K., and P. L. Stoffa (1996), Bayesian inference, Gibbs' sampler and uncertainty estimation in geophysical inversion, *Geophys. Prospect.*, *44*, 313–350.

Sylvester, J. J., G. C. Konstanzer, J. R. Rottier, G. D. Dockery, and J. R. Rowland (2001), Aegis anti-air warfare tactical decision aids, *Johns Hopkins APL Tech. Dig.*, *22*(4), 473–487.

Tarantola, A. (1987), *Inverse Problem Theory: Methods for Data Fitting and Parameter Estimation*, Elsevier Sci., New York.

P. Gerstoft and W. S. Hodgkiss, Marine Physical Laboratory, University of California, San Diego, La Jolla, CA 92093-0238, USA. (gerstoft@ucsd.edu; wsh@mpl.ucsd.edu)

M. C. Jablecki and L. T. Rogers, Atmospheric Propagation Branch, Space and Naval Warfare Systems Center, San Diego, CA 92152, USA. (jablecki@nosc.mil; trogers@spawar.navy.mil)

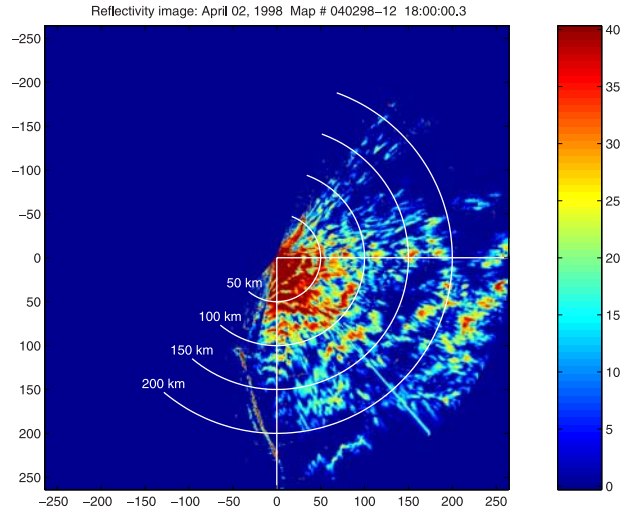

Figure 1. Clutter map (signal-to-noise ratio, measured in dB) from the SPANDAR radar corresponding to Wallops run 12. The elevation angle is 0° and E/W and N/S ranges are in kilometers.

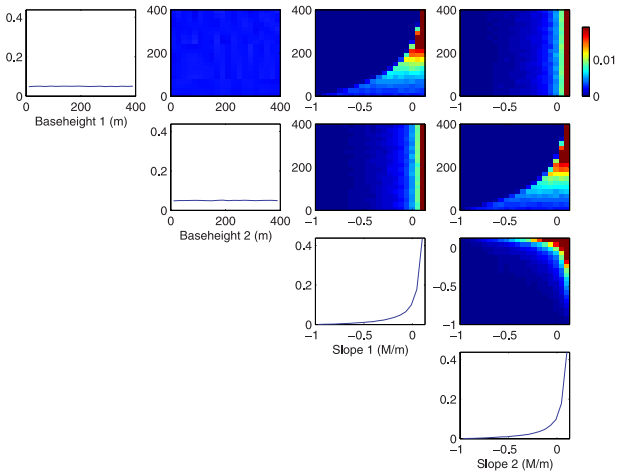

Figure 7. Prior probability distribution for the base height and slope at 0- and 100-km range. Along the diagonal the marginal for each parameter is plotted and above the diagonal show the 2-D marginals (red indicates higher probability). The distributions below the diagonal are symmetric with those above.

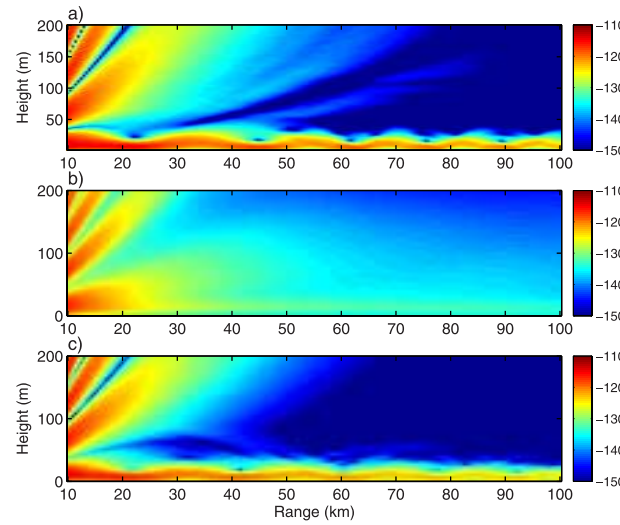

Figure 9. The propagation-loss field based on (a) the true environment (from Figure 4a), (b) prior information, and (c) posteriori information (bottom).

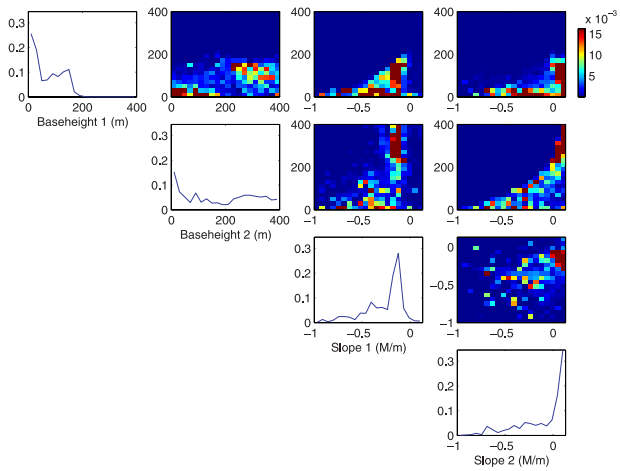

Figure 8. Posterior probability distribution for the base height and slope at 0- and 100-km range. Along the diagonal the marginal for each parameter is plotted and above the diagonal show the 2-D marginals (red indicates higher probability). The distributions below the diagonal are symmetric with those above.

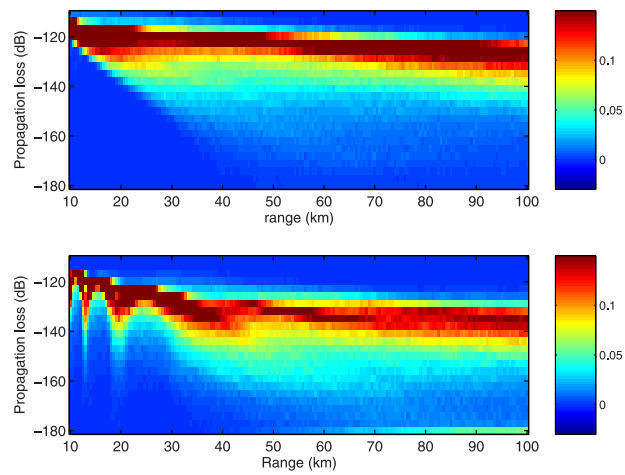

Figure 10. Prior probability distribution for propagation loss versus range at (top) 12-m and (bottom) 104-m height.

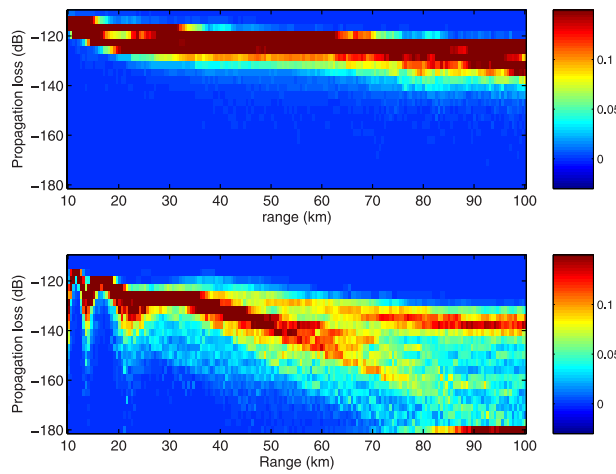

Figure 11. Posteriori probability distribution for propagation loss versus range at (top) 12-m and (bottom) 104-m height.

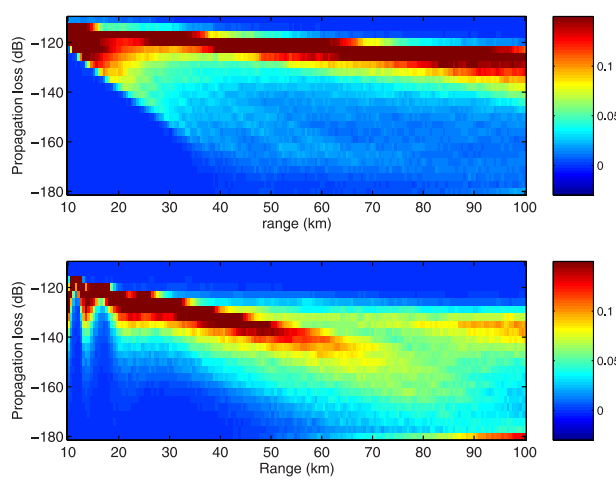

Figure 16. Posteriori probability distribution for propagation loss versus range at (top) 12-m and (bottom) 104-m height based on the 1-D marginal posterior parameter distribution in Figure 6.